Available online at www.sciencedirect.com
SCIENCE DIRECT®
Journal of Power Sources 119–121 (2003) 721–726
JOURNAL OF POWER SOURCES
www.elsevier.com/locate/jpowsour

Local structure transformation of nano-sized Al-doped $LiMn_2O_4$ sintered at different temperatures

Jyh-Fu Lee[a], Yin-Wen Tsai[b], Raman Santhanam[b], Bing Joe Hwang[b,*], Mo-Hua Yang[c], Din-Goa Liu[a]

[a]*National Synchrotron Radiation Research Center, 1 R&D Road VI, Hsinchu Science-Based Industrial Park, Hsinchu 300, Taiwan, ROC*
[b]*Microelectrochemistry Laboratory, Department of Chemical Engineering, National Taiwan University of Science and Technology, 43 Keelung Road, Section 4, Taipei 106, Taiwan, ROC*
[c]*Materials Research Laboratories, Industrial Technology Research Institute, 195-5 Chung Hsing Road, Section 4, Chutung, Hsinchu 310, Taiwan, ROC*

Abstract

$LiMn_2O_4$ and $LiAl_{0.15}Mn_{1.85}O_4$ were synthesized via the sol–gel process using citric acid as the chelating agent, followed by sintering at various temperatures. The electronic and atomic structures of $LiMn_2O_4$ and $LiAl_{0.15}Mn_{1.85}O_4$ powders were probed by means of Mn K-edge X-ray absorption spectroscopy (XAS). Al-doping was found to promote the sintering of spinel $LiMn_2O_4$ so that the degree of structural disorder around Mn atoms in $LiAl_{0.15}Mn_{1.85}O_4$ becomes lower than that of $LiMn_2O_4$, leading to an excellent capacity retention of this cathode material for lithium battery in charge–discharge cycle.

Keywords: Lithium battery; $LiMn_2O_4$; $LiAl_{0.15}Mn_{1.85}O_4$; Capacity fading mechanism; X-ray absorption spectroscopy

1. Introduction

Spinel $LiMn_2O_4$ is the most widely studied cathode material for lithium rechargeable batteries due to advantages including easy preparation, low cost, non-toxicity, and relatively high energy density [1–5]. However, a significant capacity loss of the spinel $LiMn_2O_4$ during the course of cycling prevents its extensive use [6–8]. In order to improve the electrode performance, one effective approach is to substitute a small portion of Mn ions by other dopant ions [9–13]. Recently, we have succeeded in synthesizing the Al-doped spinel ($LiAl_xMn_{2-x}O_4$) with better cycling performance [14]. At the same time, Myung et al. [15] reported that the excellent cyclability of Al-doped spinel resulted from a stabilized structure as well as reduced strain during the repeated intercalation/deintercalation of lithium. The degradation mechanism of spinel $LiAl_{0.2}Mn_{1.8}O_4$ cathode material at elevated temperatures was discussed by Sun et al. [16] based on the experimental evidence from X-ray diffraction and high-resolution transmission electron microscopy. They found that the capacity loss was attributable to the formation of tetragonal $Li_2Mn_2O_4$ and the rocksalt phase Li_2MnO_3 in the cycled electrode. Lee and coworkers [17–19] studied a series of Al-doped spinels using XRD, SEM, TEM and EPMA, and reached a similar conclusion that Al-doping always gave a better cycling performance compared to the undoped spinel $LiMn_2O_4$.

Electrochemical properties of the electrode materials strongly depended on the structural characteristics. Many of the structure–property relationships have been clarified by X-ray powder diffraction technique. However, this method provides average structural information for the crystalline phases with long-range order. Recently, X-ray absorption spectroscopy (XAS) was proved to be a powerful tool in the structural characterization of cathode materials for rechargeable lithium batteries [20–23]. The extended X-ray absorption fine structure (EXAFS) provides many quantitative short-range-order structural parameters including type and number of neighboring atoms, interatomic distance, and Debye–Waller factor [24]. On the other hand, the X-ray absorption near-edge structure (XANES) reflects the oxidation state, electronic configuration and site symmetry of the absorbing atom.

In previous charge–discharge cycling experiments, we have already shown that the capacity retention of Al-doped spinel was significantly better than that of $LiMn_2O_4$ [14].

* Corresponding author. Tel.: +886-2-2737-6624; fax: +886-2-2737-6644.
E-mail address: bjh@ch.ntust.edu.tw (B.J. Hwang).

0378-7753/03/$ – see front matter © 2003 Published by Elsevier Science B.V.
doi:10.1016/S0378-7753(03)00210-6

In order to gain deep insight into the mechanism of such an enhanced capacity retention, XAS was employed in the present work to thoroughly investigate the electronic and atomic structures of $LiMn_2O_4$ and $LiAl_{0.15}Mn_{1.85}O_4$.

2. Experimental

$LiMn_2O_4$ and $LiAl_{0.15}Mn_{1.85}O_4$ powders were synthesized using citric acid as the chelating agent. Stoichiometric amounts of lithium acetate ($Li(CH_3COO)\cdot 4H_2O$), manganese acetate ($Mn(CH_3COO)_2\cdot 4H_2O$), and aluminum nitrate ($Al(NO_3)_3\cdot 9H_2O$) were dissolved in distilled water into which citric acid was added dropwise with continuous stirring. The solution pH was adjusted to 6.0 by adding ammonium hydroxide and the temperature was maintained at 35 °C. The mixture was then heated in a water bath to 85 °C and maintained for 4 h until a transparent sol was obtained. Finally, the resultant sol precursor was ground to fine powder and sintered in different batches at various temperatures, namely, 300, 400, 500, 600, 700, and 800 °C, in oxygen for 10 h with a heating rate of 2 °C/min.

XAS experiments were carried out in transmission mode at beam line BL17C of National Synchrotron Radiation Research Center (NSRRC), Hsinchu, Taiwan. The electron storage ring was operated at an energy of 1.5 GeV with a current between 120 and 200 mA. A Si(1 1 1) double crystal monochromator was employed for energy selection. Rejection of high-order harmonic contaminations was achieved by mirrors. The intensities of the incident and transmitted beams were measured by gas ionization chambers. Energy calibration was performed against a reference Mn foil, which was measured simultaneously in each scan.

Standard procedures were followed to analyze the EXAFS data. Firstly, the raw absorption spectrum in the pre-edge region was fitted to a straight line and the background beyond the edge was fitted with a cubic spline. The EXAFS function, χ, was obtained by subtracting the post-edge background from the overall absorption and then normalized with respect to the edge jump step. The normalized χ(E) was transformed from energy space to k space, where k is the photoelectron wave vector. The $\chi(k)$ data were then multiplied by k^3 to compensate the damping of EXAFS oscillations in high-k region. Subsequently, k^3-weighted $\chi(k)$ data in the k-space ranging from 2.6 to 13.0 $Å^{-1}$ was Fourier transformed (FT) to r-space in order to separate the EXAFS contributions from different coordination shells. A nonlinear least squares algorithm was applied for curve fitting of EXAFS in r-space between 0.84 and 3.06 Å. All the computer programs were implemented in the UWXAFS 3.0 package [25] with the backscattering amplitude and the phase shift for specific atom pair theoretically calculated by using FEFF7 code [26]. The amplitude reduction factor S_0^2 was scaled to a fixed value of 0.67 after preliminary refinements. The coordination numbers (N) were also fixed to the crystallographic values since the N value is highly correlated with the Debye–Waller factor. (Note that the coordination number of the first shell Mn–O was fixed as 6 for both $LiMn_2O_4$ and $LiAl_{0.15}Mn_{1.85}O_4$, but for the second shell Mn–Mn it was fixed as 6 for $LiMn_2O_4$ and 5.55 for $LiAl_{0.15}Mn_{1.85}O_4$ to consider the small portion of Mn substituted by Al; the backscattering amplitude of photoelectron by Al is much smaller than that by Mn.)

3. Results and discussion

Fig. 1 shows the normalized XANES spectra at Mn K-edge for $LiMn_2O_4$ and $LiAl_{0.15}Mn_{1.85}O_4$ powders together with those for reference compounds Mn_2O_3 and MnO_2. The edge energies of all the $LiAl_{0.15}Mn_{1.85}O_4$ samples with various sintering temperatures were found to be lower than that of the Mn^{4+} reference (MnO_2) but higher than that of the Mn^{3+} reference (Mn_2O_3) (Fig. 1b). This evidence indicates a mixed valence of Mn (Mn^{3+}/Mn^{4+}) in all of the Al-doped samples. Nevertheless, a slightly lower edge energy was observed on the sample sintered at 300 °C than on other samples sintered at higher temperatures. In contrast, the edge energy for the undoped $LiMn_2O_4$ sample sintered at 300 °C is lower than that of Mn^{3+} reference (Fig. 1a), indicating that a significant portion of Mn ions in this sample remained in the +2 oxidation state. Once the sintering temperature was elevated to above 400 °C, the average Mn valence increased to a stable value between +3 and +4.

Fourier transformation of EXAFS gives the radial distribution function, as shown in Fig. 2. The first peak in Fig. 2 corresponds to the contribution from the first shell Mn–O, and the second peak represents a Mn–Mn/Al contribution from the second shell. It can be seen that variation in the intensity of the Mn–O peak was quite small among the samples of same series with different sintering temperatures. This observation reveals that a stable [MnO_6] octahedral coordination environment was formed even at a sintering temperature as low as 300 °C. Higher sintering temperatures did not give rise to any obvious difference in the first shell coordination. On the other hand, significant variation in the Mn–Mn/Al peaks appeared as a function of sintering temperature. The variation in peak intensity for undoped $LiMn_2O_4$ was greater than that of $LiAl_{0.15}Mn_{1.85}O_4$, indicating that an increased sintering temperature was more in leading to a higher structural order of the undoped $LiMn_2O_4$ than in the case of $LiAl_{0.15}Mn_{1.85}O_4$. Since Al-doping promotes the sintering of $LiMn_2O_4$, more ordered spinel structures in $LiAl_{0.15}Mn_{1.85}O_4$ materials can be formed at lower sintering temperatures. Consequently, the change in the Mn–Mn/Al peak intensity of $LiAl_{0.15}Mn_{1.85}O_4$ with increased sintering temperature, occurs to a relatively less extent than that for undoped $LiMn_2O_4$.

Detailed data analysis for the first two Fourier transform peaks was performed by curve fitting with two different models, two- and three-shell models. In the two-shell model, the coordination number for the oxygen atoms in the first

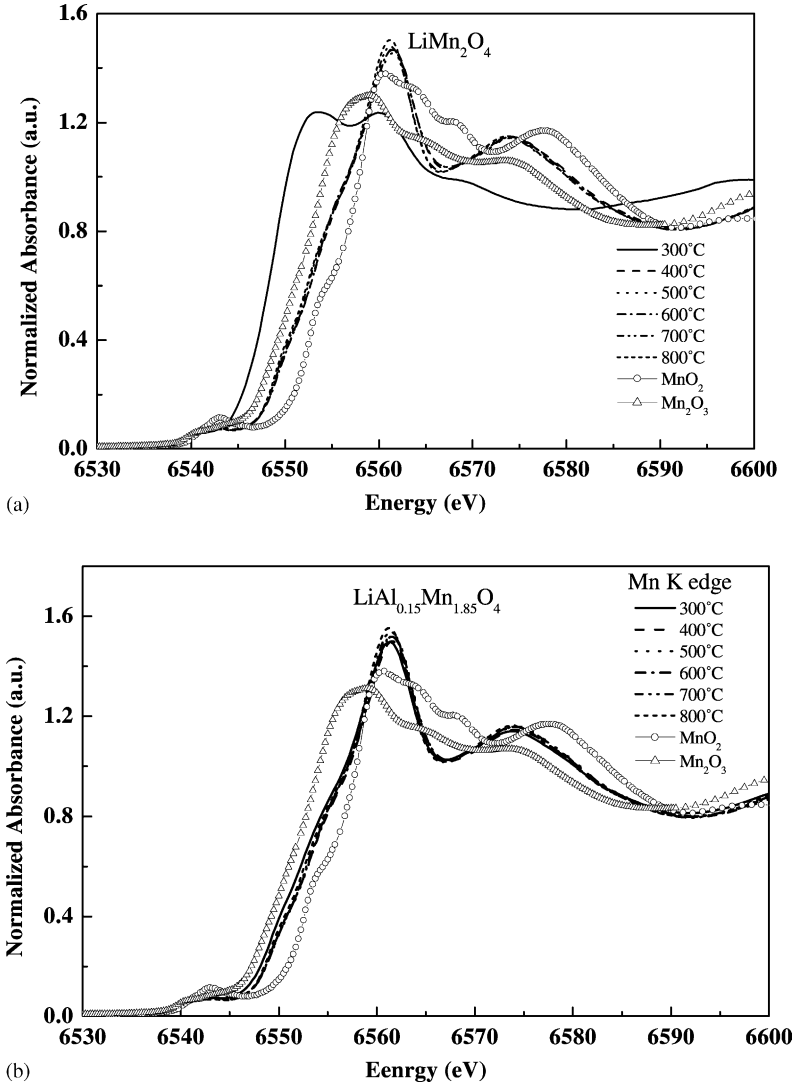

Fig. 1. Normalized at XANES spectra Mn K-edge for (a) $LiMn_2O_4$, and (b) $LiAl_{0.15}Mn_{1.85}O_4$ powders as a function of sintering temperature. The spectra of reference compounds MnO_2 and Mn_2O_3 are also shown for comparison.

Mn–O shell was fixed to the crystallographic value of 6 for all samples. Moreover, all the six Mn–O bond lengths in [MnO_6] octahedron are considered to be the same. The second shell consists of Mn atoms in the neighboring 16*d* octahedral sites with the coordination number fixed to 6 for $LiMn_2O_4$ and 5.55 for $LiAl_{0.15}Mn_{1.85}O_4$ because a small portion of Mn atoms is substituted by Al atoms, which also occupy some of the 16*d* octahedral sites. However, in three-shell model, two types of Mn–O bonds are considered. One is Mn–O(4) and the other is Mn–O(2). The Mn–Mn/Al interaction becomes the third shell contribution in this model.

Structural parameters from curve fitting analysis by the two-shell model are listed in Table 1. The Mn–O distance and the Debye–Waller factor (accounting for the structural disorder) for the first shell of both undoped and Al-doped $LiMn_2O_4$ were not subject to significant changes with different sintering temperatures. This evidence can be ascribed to the formation of stable [MnO_6] octahedra at low sintering temperature. Similarly, the sintering temperature exhibited a negligible effect on the second shell Mn–Mn distance. However, remarkable variations were observed in Debye–Waller factors as a function of sintering temperature both for undoped and Al-doped $LiMn_2O_4$ samples, as shown in Fig. 3. It is also interesting to note that the Debye–Waller factors for $LiAl_{0.15}Mn_{1.85}O_4$ were relatively smaller than the corresponding values for $LiMn_2O_4$ at all sintering temperatures. Two possible mechanisms were proposed to explain such an observation. The first one is the enhancement of sintering of $LiMn_2O_4$ by Al-doping, which can increase the structural ordering even at low sintering temperatures. The other one is related to the substitution of some Jahn–Teller active Mn^{3+} ions by Al^{3+} ions, which can diminish the Jahn–Teller distortion and hence result in greater structural stability. Another point worth mentioning is that the second-shell Debye–Waller factor of $LiMn_2O_4$ decreased faster than

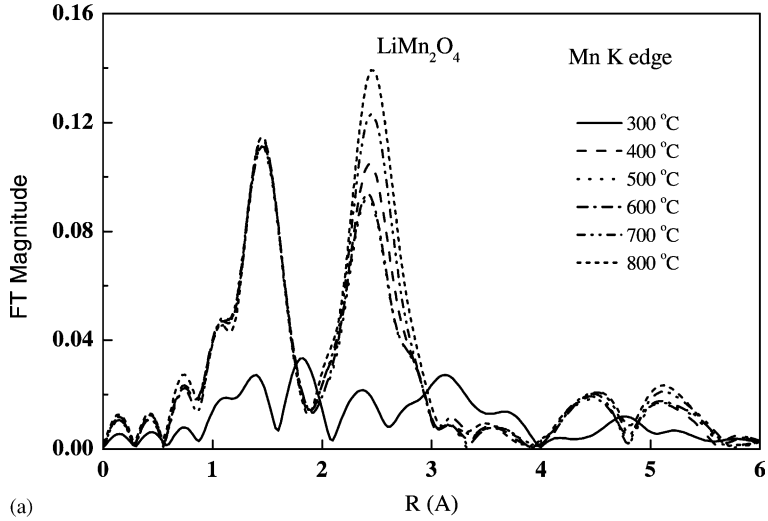

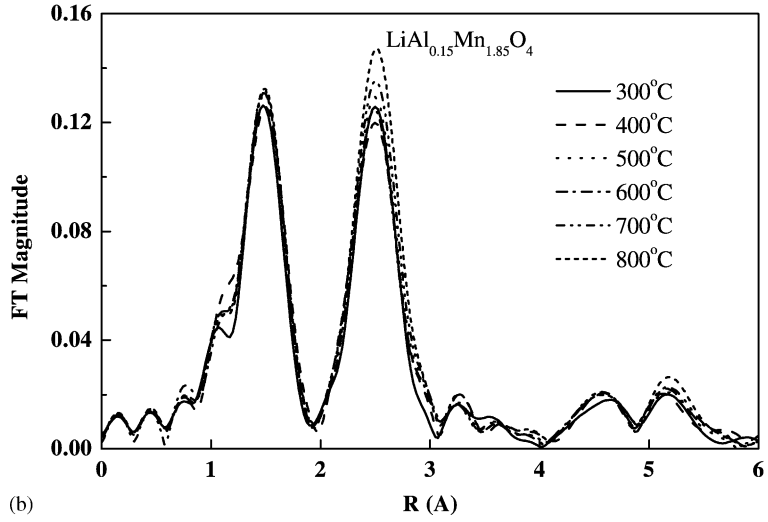

Fig. 2. Fourier transforms of the Mn K-edge EXAFS spectra as a function of sintering temperature for (a) $LiMn_2O_4$, and (b) $LiAl_{0.15}Mn_{1.85}O_4$ powders.

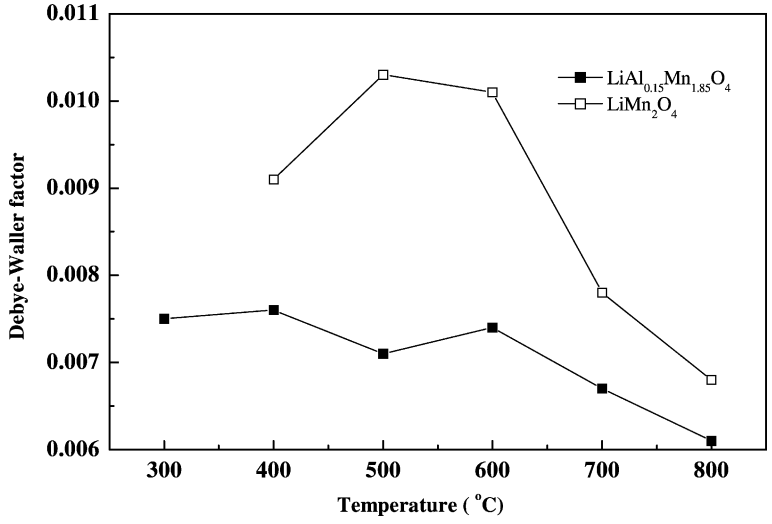

Fig. 3. Debye–Waller factors for the second shell Mn–Mn as a function of sintering temperature for undoped and Al-doped $LiMn_2O_4$.

that of $LiAl_{0.15}Mn_{1.85}O_4$ with increasing sintering temperature, implying the formation of a more ordered structure in the case of $LiAl_{0.15}Mn_{1.85}O_4$ at low sintering temperatures.

The structural parameters were also obtained by curve fitting analysis by using the three-shell model. The coordination distances, and the Debye–Waller factors obtained from this model are almost similar to that of the values obtained from two-shell model. However, significant differences were observed between the *R*-factors obtained from two- and three-shell models as a function of the sintering temperature for undoped and Al-doped $LiMn_2O_4$ samples, as shown in Fig. 4a and b, respectively. It can be seen that the *R*-factors for $LiAl_{0.15}Mn_{1.85}O_4$ were relatively smaller than the corresponding values of $LiMn_2O_4$ at all sintering temperatures. It is also interesting to note that the difference in *R*-factors obtained from both the models is very low for $LiAl_{0.15}Mn_{1.85}O_4$ (Fig. 4b), however, the difference is very high in the case of $LiMn_2O_4$ (Fig. 4a). This observation is related to the distortion caused by the presence of Jahn–Teller active Mn^{3+} ions in $LiMn_2O_4$.

On the whole, the Debye–Waller factor and *R*-factors were successfully used to evaluate the performance of the cathode materials for lithium batteries in this study. From the results of EXAFS data analysis, one can see that Al-doping leads to lower local structural disorder on sintering as compared to that of undoped $LiMn_2O_4$. Lower local disorder observed in the case of $LiAl_{0.15}Mn_{1.85}O_4$ would provide space to accommodate the Jahn–Teller distortion and lead to fast lithium ion insertion/extraction reactions. Recently, the relationship between the local disorder and capacity fading have been reported by various authors for Co-substituted $LiMn_2O_4$, Al-substituted $LiCoO_2$, and $Li_{1.5+x}Na_{0.5}MnO_{2.85}I_{0.12}$ [23,27,28]. Hence, the excellent capacity retention of $LiAl_{0.15}Mn_{1.85}O_4$ observed in cycling experiments is

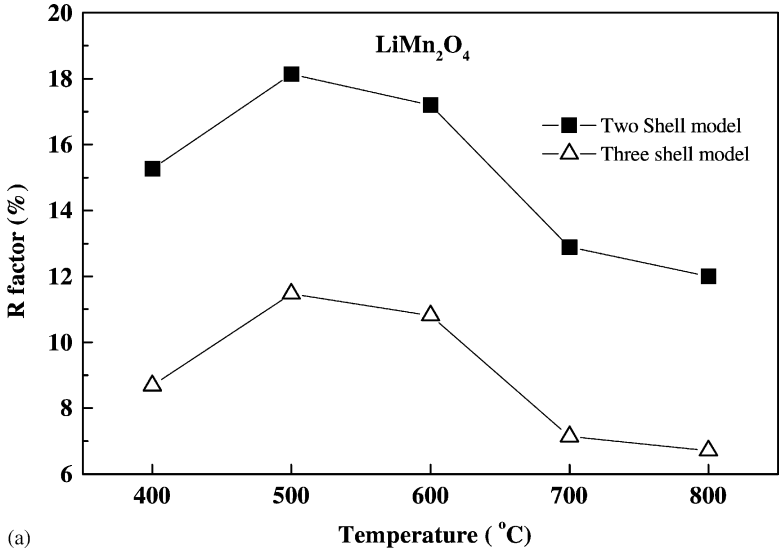

(a)

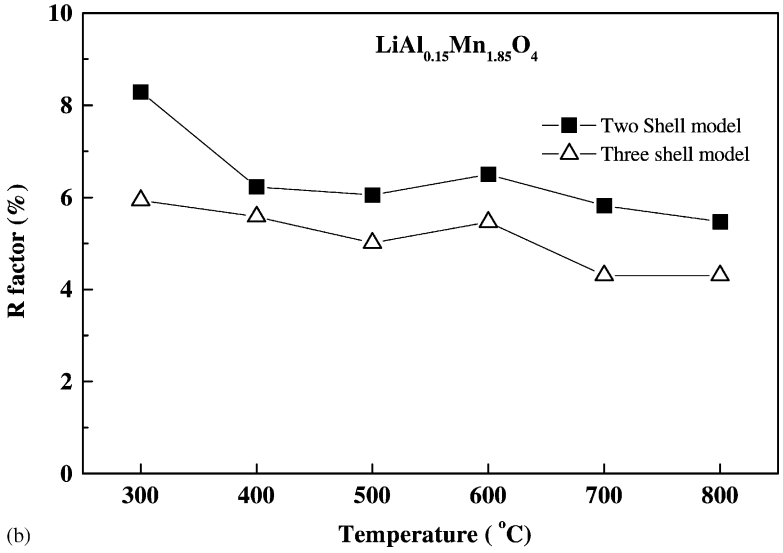

(b)

Fig. 4. *R*-factors obtained from two- and three-shell models for (a) undoped, and (b) Al-doped $LiMn_2O_4$ as a function of sintering temperature.

Table 1
Computer-fitted EXAFS parameters for $LiMn_2O_4$ and $LiAl_{0.15}Mn_{1.85}O_4$ with various sintering temperatures[a]

Temperature (°C)	Shell	N	R (Å)	σ^2 (Å^2)	ΔE_0 (eV)
$LiMn_2O_4$					
400	Mn–O	6	1.926	0.0076	−6.1
	Mn–Mn	6	2.899	0.0091	−10.9
500	Mn–O	6	1.927	0.0078	−6.1
	Mn–Mn	6	2.893	0.0103	−11.6
600	Mn–O	6	1.927	0.0077	−6.2
	Mn–Mn	6	2.893	0.0101	−11.9
700	Mn–O	6	1.930	0.0077	−6.4
	Mn–Mn	6	2.909	0.0078	−11.2
800	Mn–O	6	1.929	0.0077	−6.6
	Mn–Mn	6	2.914	0.0068	−10.8
$LiAl_{0.15}Mn_{1.85}O_4$					
300	Mn–O	6	1.912	0.0066	−2.8
	Mn–Mn	5.55	2.900	0.0075	−5.3
400	Mn–O	6	1.915	0.0060	−2.5
	Mn–Mn	5.55	2.896	0.0076	−5.5
500	Mn–O	6	1.912	0.0060	−2.8
	Mn–Mn	5.55	2.898	0.0071	−5.4
600	Mn–O	6	1.912	0.0060	−2.9
	Mn–Mn	5.55	2.897	0.0074	−5.8
700	Mn–O	6	1.915	0.0060	−2.9
	Mn–Mn	5.55	2.902	0.0067	−5.5
800	Mn–O	6	1.916	0.0059	−2.9
	Mn–Mn	5.55	2.908	0.0061	−5.3

[a] *Note*: N is the coordination number (constrained to the crystallographic value), R the average interatomic distance, σ^2 the Debye–Waller factor, and ΔE_0 the inner potential correction.

attributable to the highly ordered local atomic environment around the Mn atom in the lattice.

4. Conclusions

$LiMn_2O_4$ and $LiAl_{0.15}Mn_{1.85}O_4$ powders were synthesized via the sol–gel process using citric acid as the chelating agent, followed by sintering at various temperatures. From the observation of the Mn K-edge EXAFS spectra of these materials, it was found that Al-doping can promote the sintering of the spinel $LiMn_2O_4$. The structural disorder of neighboring atoms (particularly for the second shell) around Mn atom is greater in $LiMn_2O_4$ than for $LiAl_{0.15}Mn_{1.85}O_4$. This is in part attributable to the diminution of the Jahn–Teller distortion in the latter case. Accordingly, the excellent capacity retention of $LiAl_{0.15}Mn_{1.85}O_4$ during charge–discharge cycles seems strongly related to lower local structural disorder compared to that of $LiMn_2O_4$.

Acknowledgements

The financial support from National Science Council (NSC 89-2214-E-011-044 and NSC 90-2811-E-011-005) and Education Ministry (EX-91-E-FA09-5-4), National Synchrotron Radiation Research Center (NSRRC) and National Taiwan University of Science and Technology is gratefully acknowledged.

References

[1] S. Megahed, B. Scrosati, J. Power Sources 51 (1994) 79.
[2] J.M. Tarascon, E. Wang, F.K. Shokoohi, W.R. Mckinnon, S. Colson, J. Electrochem. Soc. 138 (1991) 2859.
[3] T. Ohzuku, M. Kitagawa, T. Hirai, J. Electrochem. Soc. 137 (1990) 769.
[4] J.M. Tarascon, D. Guyomard, J. Electrochem. Soc. 138 (1991) 2864.
[5] M.M. Thackeray, Prog. Solid State Chem. 25 (1997) 1.
[6] J.M. Tarascon, F. Coowar, G. Amatucci, F.K. Shokoohi, D.G. Guyomard, J. Power Sources 54 (1995) 103.
[7] P. Barboux, J.M. Tarascon, F.K. Shokoohi, J. Solid State Chem. 94 (1991) 185.
[8] S. Bach, M. Henry, N. Baffier, F.K. Shokoohi, J. Solid State Chem. 88 (1990) 25.
[9] Y. Ein-Eli, J.T. Vaughty, M.M. Thackeray, S. Mukerjee, X.Q. Yang, J. McBreen, J. Electrochem. Soc. 146 (1999) 908.
[10] J.H. Lee, J.K. Hong, D.H. Jang, Y.K. Sun, S.M. Oh, J. Power Sources 89 (2000) 7.
[11] G.X. Wang, D.H. Bradhurst, H.K. Liu, S.X. Dou, Solid State Ionics 120 (1999) 95.
[12] N. Hayashi, H. Ikuda, M. Wakihara, J. Electrochem. Soc. 146 (1999) 1351.
[13] Y. Ein-Eli, W.F. Howard, J. Electrochem. Soc. 144 (1997) L205.
[14] B.J. Hwang, R. Santhanam, D.G. Liu, Y.W. Tsai, J. Power Sources 102 (2001) 326.
[15] S.T. Myung, S. Komaba, N. Kumagai, J. Electrochem. Soc. 148 (2001) 482.
[16] Y.K. Sun, C.S. Yoon, C.K. Kim, S.G. Yoon, Y.S. Lee, M. Yoshio, I.H. Oh, J. Mater. Chem. 11 (2001) 2519.
[17] Y.S. Lee, H.J. Lee, M. Yoshio, Electrochem. Commun. 3 (2001) 20.
[18] Y.S. Lee, M. Yoshio, Electrochem. Solid State Lett. 4 (2001) 85.
[19] Y.S. Lee, M. Yoshio, Electrochem. Solid State Lett. 4 (2001) 155.
[20] R.S. Liu, L.Y. Jang, J.M. Chen, Y.C. Tsai, Y.D. Hwang, R.G. Liu, J. Solid State Chem. 128 (1997) 326.
[21] B. Ammundsen, D.J. Jones, J. Rozeire, J. Solid State Chem. 141 (1998) 294.
[22] P. Aitchison, B. Ammundsen, D.J. Jones, G. Burns, J. Rozeire, J. Mater. Chem. 9 (1999) 3125.
[23] C.R. Horne, U. Bergmann, J. Kim, K.A. Striebel, A. Manthiram, S.P. Cramer, E.J. Cairns, J. Electrochem. Soc. 147 (2000) 395.
[24] B.J. Hwang, R. Santhanam, C.P. Huang, Y.W. Tsai, J.F. Lee, J. Electrochem. Soc. 149 (2002) 694.
[25] E.A. Stern, M. Newville, B. Ravel, Y. Yacoby, D. Haskel, Phys. B 208–209 (1995) 117.
[26] S.I. Zabinsky, J.J. Rehr, A. Ankudinov, R.C. Albers, M.J. Eller, Phys. Rev. B 52 (1995) 2995.
[27] P. Aitchison, B. Ammundsen, D.J. Jones, G. Burns, J. Roziere, J. Mater. Chem. 9 (1999) 3125.
[28] W.S. Yoon, K.K. Lee, K.B. Kim, J. Electrochem. Soc. 149 (2002) A146.